Experimental analysis of timber inclusions effect on paraseismic behavior of earth masonry walls

Jairo Aranguren, Florent Vieux-Champagne, Maïa Duriez, Jean-Emmanuel Aubert

Experimental analysis of timber inclusions effect on paraseismic behavior of earth masonry walls

Jairo Aranguren[1], Florent Vieux-Champagne[2], Maïa Duriez[3] and Jean-Emmanuel Aubert[4]

Abstract. This research aims at the seismic assessment and understanding of a traditional loadbearing system incorporating horizontal timber elements into earth brick masonry walls. In order to characterize the global behavior of the loadbearing device, an experimental campaign was performed on the constituents (i.e. bricks and mortar) and on masonry samples. Compression tests were carried out on four geometries of earth brick samples and three geometries of earth mortar samples. As the methods to obtain the compressive strength of earth material are still discussed within the scientific community, a focus was made on different configurations tested. Uniaxial compression tests were performed on two earth brick wallets. Then, two brick walls (with and without horizontal timber reinforcement) were submitted to lateral quasi-static cyclic load. A LVDTs system and a stereo correlation image system were coupled to study the experimental response of the reinforced and unreinforced walls. This investigation led to estimate the lateral strength, the stiffness degradation and the dissipated energy of both reinforced and unreinforced masonry walls. Moreover, it allowed the comparison between the failure modes of the two types of wall. This analysis brings light on the mechanical impact of the horizontal reinforcement.

Keywords: Seismic behavior, traditional loadbearing system, earth brick masonry, timber insertions, stereo correlation image system, timber laced masonry.

1 Introduction

Traditional masonry structures represent an important part of the buildings around the world. This can be explained in particular by the constructive advantages of this system against other structure typologies such as reinforced concrete (RC) in terms of: construction costs, execution complexity and speed, materials accessibility and workmanship qualification requirements. Despite being commonly present in areas where the seismic risk is high (e.g. Nepal, Pakistan, Turkey, Italy, Haiti, etc.), traditional masonry structures are especially vulnerable when subjected to lateral loading such as seismic stresses. This was particularly clear after 2015's earthquake in Gorkha, Nepal, where thousands of non-engineered masonry dwellings suffered collapse and/or severe damage, affecting thousands of families and households. More details about the post-seismic construction in Nepal are available in [1].

1 Laboratoire Matériaux et Durabilité des Constructions (LMDC), Université de Toulouse, UPS, INSA, 135 avenue de Rangueil, 31077 Toulouse Cedex 4, France, e-mail : jairodavidbz@gmail.com

2 Univ. Grenoble Alpes, CNRS, Grenoble INP, 3SR, 38000 Grenoble, France, e-mail : florent.vieux-champagne@univ-grenoble-alpes.fr

3 Laboratoire Matériaux et Durabilité des Constructions (LMDC), Université de Toulouse, UPS, INSA, 135 avenue de Rangueil, 31077 Toulouse Cedex 4, France, e-mail : maia.duriez@insa-toulouse.fr

4 Laboratoire Matériaux et Durabilité des Constructions (LMDC), Université de Toulouse, UPS, INSA, 135 avenue de Rangueil, 31077 Toulouse Cedex 4, France, e-mail : aubert@insa-toulouse.fr

As remarked by different authors [2]-[3], the collapse of masonry structures is mainly associated with material and construction deficiencies, as well as the lack of wall-to-wall and roof-to-wall connections and the presence of heavy roofs. However, replacement of existing dwellings with new structures built according to paraseismic standards used in developed countries is not appropriate because of the high cost and embodied energy. On the contrary, the challenge today is either to build new structures based on the improvement of vernacular constructions, or to be able to reinforce existing structures by using local resources according to the local building culture.

This article provides a structural analysis regarding the paraseismic behavior of the interesting system of timber laced masonry since it is a traditional technique that seems to be specifically developed in seismic prone areas such as Nepal, as well as in Greece, Turkey and India (see [3]-[6]). This system is characterized by stone or earth masonry reinforced with horizontal timber beams in most cases (cf. **Fig. 1**).

By combining a rigid material (masonry) with a flexible material (timber) it is possible to modify the behavior of masonry making it more flexible and more ductile. This composite system allows increasing the energy dissipation capacity of walls subjected to lateral forces thanks to the combined effect of both the friction on the joints, and on the timber and the masonry elements interface. The absorption of large amounts of energy is also favored as inclusions interrupt structural homogeneity allowing relative displacements of the sub-divided elements [3]. The inclusions also play a fundamental role in controlling the crack propagation, since they allow holding masonry together when subjected to seismic forces, facilitating the formation of numerous micro and macrocracks before rupture [5]. Moreover, it has been found that inclusions may increase the masonry compressive strength as they act as confinement reinforcement for masonry [6].

Despite the popularity of masonry reinforced with timber, the lack of scientific knowledge regarding this system is an important hindrance to its use and more widely to its sustainability. Indeed, very little literature is available [6] despite the complexity of the behavior of this kind of structure. Moreover, the great variability of masonry structures makes elaboration of a representative constitutive law difficult. Therefore, research considers the study of structures with very specific materials and constructive arrangements for which different theoretical, experimental and numerical approaches are proposed.

This research follows two main objectives; first, to increase the scientific knowledge on seismic behavior of traditional adobe masonry structures and secondly, to assess the influence of a specific masonry loadbearing system adapted to traditional construction techniques and vernacular materials, on the masonry's seismic behavior.

The purpose of this research is to study the influence of the timber inclusion in a part of masonry. The influence of specific vernacular earthquake resistant technologies at the scale of masonry structures (confining effect, tie effect, out-of-plane behavior and geometrical aspects) have been detailed in other studies (cf. [6]-[7], [11]-[13]).

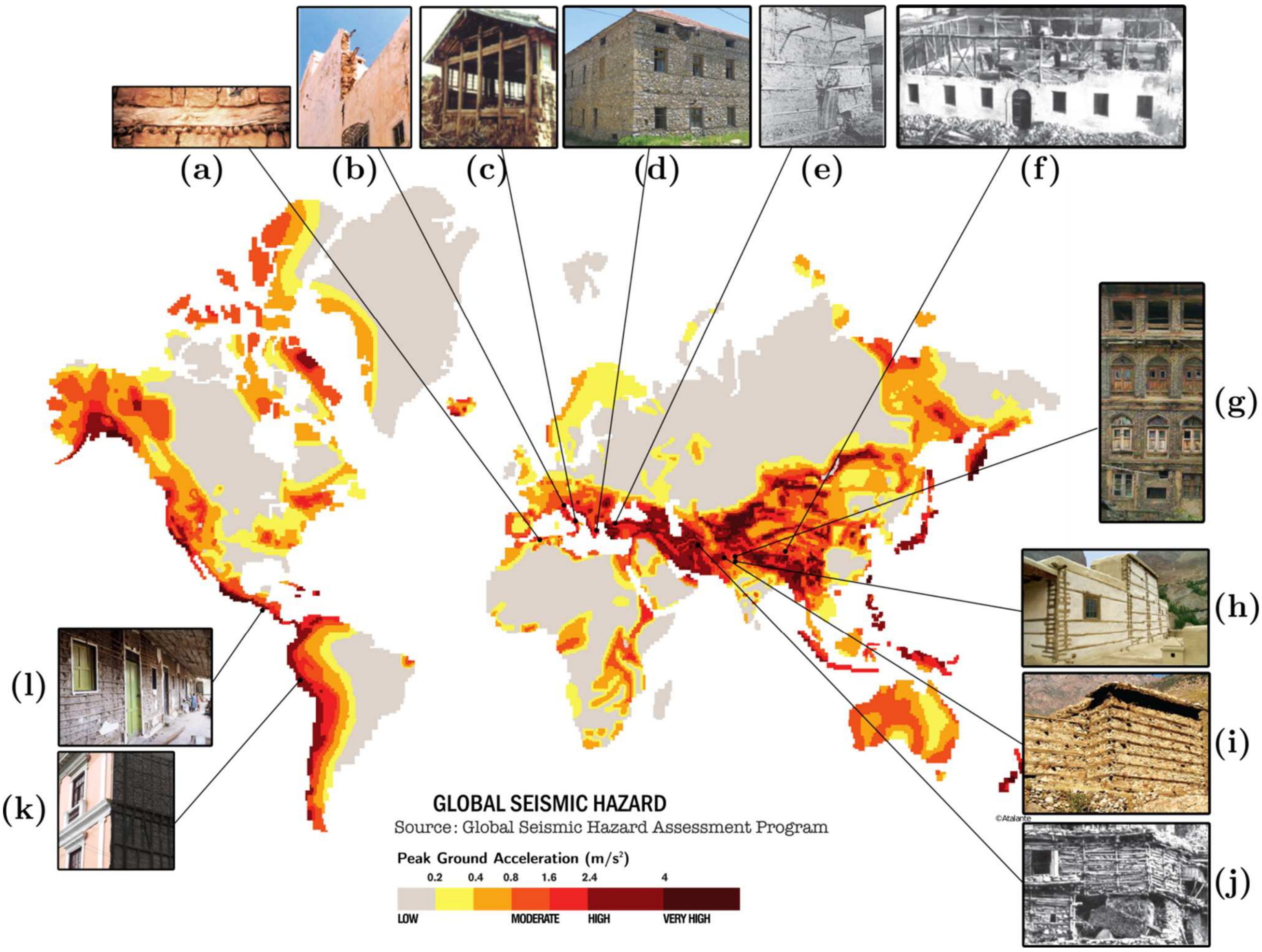

Fig. 1 Timber frame structures in the world (Adapted from [7]) : (a-b) Media Corpus (seen in [8]), (c) Tsakanika-Theohari (seen in [8]), (d) Hoffman (seen in [8]) (e) Aytun (seen in [8]) (f) Liu [9], (g) Langenbach [5], (h) Hoffman (seen in [8]), (i) Schacher (seen in [8]), (j) Wutt (seen in [8]), (k) Langenbach [10], (l) T. Joffroy (seen in [7])

The studied structure is made of earth masonry walls reinforced with horizontal ladder shaped timber ties. An experimental campaign was performed from the scale of the masonry elements (bricks and mortar) to the scale of a shear wall of about 1.3m × 1.3m. On the first scale, a focus is made on different compression tests since there is still an important discussion on earth material as no consensus exists regarding the procedure to determine the mechanical characteristics of earth bricks. On a second scale, the masonry compression behavior is studied through compression tests carried on masonry wallets. On the scale of the wall, results of lateral quasi-static load tests on two adobe walls (with and without timber bands) and the efficiency of reinforcement are discussed.

In order to characterize the traditional Nepalese masonry system the experimental program includes; bending and uniaxial compression tests on the constituents (bricks and mortar), compression tests on masonry wallets and quasi-static lateral loading tests on masonry walls. The current paper presents the materials, the test procedures and the experimental results for each test achieved on masonry elements (bricks and mortar), scale wallets and scale walls.

The dimensions of the materials and elements adopted within the framework of this project were chosen to be representative of the *Design catalogue for reconstruction of earthquake resistant houses* in Nepal [14]. This document, prepared by the government of Nepal as a response to the earthquake on 15th April 2015, aims at presenting the minimal specifications necessary to reconstruct masonry dwellings using traditional paraseismic techniques, which guarantee the vernacular architecture conservation. Variability of materials used to fabricate earth bricks and timber elements of vernacular buildings is significant since it is common practice to dispose of materials locally available. However, all earthen materials show similar mechanical characteristics because of their capillarity properties. In this respect, earth and wood used for this project were local products. It is worth to highlight that the indications provided in the catalogue were completed with other documents dealing with construction practices in Nepal (see [8], [15]).

2 Constituents of masonry

Masonry is a complex composite material. In order to properly understand its behavior, it is necessary to characterize the main mechanical properties of its constituents (bricks and mortar). This paragraph focuses on the determination of compressive and tensile strengths of both mortar and units. These properties will be useful to understand the behavior of the masonry at the scale of the wallet (cf. part 3).

2.1 Materials and experimental setup

Bricks and mortar used for the experiments were supplied by a local manufacturer of earthen products. Earth bricks were manufactured by extrusion (without compression) and by air drying with a size of $50 \times 105 \times 220\ \mathrm{mm}^3$. Mortar was composed of a mixture of earth laminated at 0.7 / 0.1 mm and white sand 0 / 4 mm. Earth was composed of quartz, calcite, goethite, feldspars, illite and montmorillonite [16]. The binder was prepared from a mixture of water and earth in proportions of approximately $1:6$. Timber used as reinforcement is made of raw unplanted fir tree, untreated, class C18 according to the standard NF EN 338 [17].

Since the compressive characterization of earth bricks is still under discussion (see [18]-[19]), four protocols were implemented to determine the compressive strength of masonry units. Two tests were performed on entire bricks according to standard NF EN 772-1 [20]; for the first panel, entire bricks were tested in horizontal position (load applied on bed joints) (cf. **Fig. 2(a)**); for the second panel, entire bricks were tested in vertical position (load applied on head joints). Additionally, a third type of tests was performed on stacked half-bricks considering the prescriptions of the experimental standard XP P13-901 (2001) [21]. However, unlike standard, a fine layer of sand was laid out between the half-bricks, and on the top and bottom surface of each specimen to ensure a uniform load distribution. A fourth protocol was used on samples formed by superimposing four half-bricks, in order to guarantee an aspect ratio of 2 (cf. **Fig. 2(b)**). The tensile strength was determined indirectly through 3-point bending tests on entire bricks. The Young's modulus and Poisson's ratio were obtained through a series of uniaxial compression tests performed on entire bricks vertically positioned. Loads were applied according to prescriptions in NF EN 12390-13 [22]. Additionally, compression tests on three types of earth mortar samples with different aspect ratios were carried out. For the first panel (aspect ratio of 1), mortar specimens with a size of 40 × 40 × 160 mm^3 were tested according to EN 1015-11 [23] (cf. **Fig. 2(c)**). For the second panel (aspect ratio of 1.7) samples with initial dimensions of 40 × 40 × 160 mm^3 were cut in two halves. Then, the cut specimens were tested along the largest direction. The last panel (aspect ratio of 4) consisted of specimens of size 40 × 40 × 160 mm^3 tested along the largest dimension (cf. **Fig. 2(d)**). Furthermore, mortar tensile strength was obtained through 3-point bending tests according to EN 1015-11.

(a) **(b)** **(c)** **(d)**

Fig. 2 Compression tests on: (a) vertical entire bricks, (b) 4 stacked half-bricks, (c) mortar aspect ratio 1, (d) mortar aspect ratio 4.

2.2 Results

Tests results are shown in **Table 1**. For each configuration, mean values and standard deviation SD (%) are presented. Before each test, samples were measured and weighted, which allows to calculate the brick bulk density ρ = 2098 kg/m^3 ($SD = 2.4$ %) and the mortar bulk density ρ = 1918 kg/m^3 ($SD = 0.6$ %).

Observations carried out after compression tests on stacked half-bricks revealed the presence of an unconfined zone in the sand layers, where the load was only partially transferred between bricks. Therefore, the surface used to determine brick compression strength of stacked half-bricks is reduced by 10 % on each side to obtain an equivalent confined area. This reduction percentage was determined empirically.

The higher compressive strength corresponds to entire bricks tested horizontally. This is essentially due to the specimen geometrical conditions. As exposed by different authors [18]-[19], [26]-[28], compressive strength increases with decreasing aspect ratio because of the confinement produced by the friction between the surfaces of the samples and the press plates. This friction can induce inconsistent results as shown by [29]. The compressive strength obtained from tests on 2 and 4 stacked half-bricks is quite similar. However, these values are substantially lower than the strength found in tests on entire bricks. This difference can probably be explained by the fact that the sand has a higher Poisson's ratio, which caused high lateral strain under compression inducing some tensile stress on the bricks. This fact could be at the origin of the failure mode observed on stacked specimens, which is characterized by vertical cracks passing through bricks and vertical decohesion. The ones tested vertically (cf. **Fig. 2 (a)**) present the typical compression failure mode (two opposite confinement cones) and a compressive strength between that of bricks tested horizontally and stacked samples. The variability of compressive strength is significantly higher when testing 2 stacked half-bricks ($SD = 25.3$ %). Conversely, tests on entire vertical bricks are considerably more consistent as they report the lowest standard deviation (10.9 %). Furthermore, taking the results of the tests on entire vertical bricks as a reference, it appears that the mean value of the bricks tensile strength (measured in flexion) corresponds to 17 % of the compressive strength.

Table 1. Mechanical parameters of the constituents

Material	Mechanical parameter		Number of tests	Mean	SD (%)
Brick	Compressive strength (MPa)	Entire block horizontal	6	10.9	14.4
		Entire block vertical	6	7.7	10.9
		2 stacked half-bricks	7	4.9	25.3
		4 stacked half-bricks	6	4.8	13.6
	Tensile strength (measured in flexion) (MPa)		6	1.3	16.1
	Young's modulus (MPa)		3	4362	9.3
	Poisson's ratio (-)		2	0.12	-
Mortar	Compressive strength (MPa)	Aspect ratio 1	5	2.2	3.9
		Aspect ratio 1.7	5	1.9	6.4
		Aspect ratio 4	6	1.8	3.3
	Tensile strength (measured in flexion) (MPa)		5	0.9	9.5

Results in **Table 1** show that the mortar compressive strength is lower for higher aspect ratios. However, specimens with an aspect ratio of 1.7 and 4 exhibit similar mechanical strengths due to the fact that both samples present shear failure, as brought to light by the presence of a characteristic shear fracture surface, with sliding planes inclined 45° with respect to the vertical plane (cf. **Fig. 2(d)**). In fact, when calculating the shear strength analytically with the hypothesis of a shear fracture plane at 45° we obtain a shear strength of 0.9 MPa, which is similar to tensile strength. On the contrary, the samples with an aspect ratio of 1 revealed a typical compressive failure mode (cf. **Fig. 2(c)**). The tensile strength, measured in flexion, is about 0.9 MPa. This value corresponds to 41 % of the compressive strength found for the cubic sample.

One can suppose from **Table 1** that the behavior of the current masonry has a compression strength governed by the mortar behavior since this material has a low resistance compared to the bricks. However, this might not be the only determinant parameter as will be discussed on the masonry wallets study.

3 Masonry wallets

3.1 Materials and experimental setup

Two masonry wallets of size $525 \times 445 \times 105\ \mathrm{mm}^3$ (MC-1) and $570 \times 450 \times 105\ \mathrm{mm}^3$ (MC-2) were constructed to be tested under quasi-static uniaxial compression loading in order to analyze the behavior of the structure (rigidity, plasticity, strength, crack pattern) and to estimate the vertical load that should be applied on the elements of shear wall during the quasi-static test. The wallets were built on steel plates following a "stretcher" bond (cf. **Fig. 3(a)**). After construction, both specimens were stored in a room under ambient temperature and humidity conditions (approximately 22°C and 40% RH).

The compressive strength and the Young's modulus of the masonry were determined according to EN 1052-1. To determine the Young's modulus, the samples were subjected to three charge-discharge cycles. For each cycle, the vertical load was gradually varied between two values corresponding to a minimum pre-load of 15 kN and a load equal to 50 % of the expected masonry strength, this value was obtained from the literature [27]. Vertical and horizontal displacements were measured using Linear Variable Displacement Transformers (LVDTs) glued on one side of each wallet (cf. **Fig. 3(a)**). Once the charge-discharge cycles completed, each specimen was subjected to an increasing monotonic compression load until failure in order to determine the compressive strength.

(a) **(b)**

Fig. 3 Compression test on masonry. (a) Position of LVDT captors, (b) Stereoscopique system disposition.

A stereoscopic system was set up to visualize the compression test in order to obtain the displacement field of the MC-2 sample (cf. **Fig. 3(b)**). A system of two AVT Manta 504B cameras with 8 mm lenses was used to record the sample. Because of the uniform color of the earth bricks, a mouchetis was made on one of the faces of the wall to generate a very contrasting pattern to improve the results of the Digital Image Correlation (DIC) process. The observed face of the specimen was first painted white and then small black spots were applied using a spray gun. A LED continuous lighting system was installed to ensure a uniform light intensity on the sample. Images were taken every 10 seconds for a total of 256 images recorded during the cyclic test and 71 images obtained during the monotonic test. In a post-processing phase the recorded images were analyzed using the VIC-3D software. Displacement and deformation fields of the wallet were obtained by comparing the images of its surface acquired before and after deformation. The value of the displacement of a point corresponds to the average value of the displacement of a subset (a portion of a reference image) centered at the considered point. To determine the displacement suffered by the subset after deformation, the subset in the reference image "moves" to find a pattern that fit the best in the distorted image. The evaluation of the correspondence between the two images (normal and deformed) is done by minimizing a function that represents the intensity of gray level of the pixels contained in the subsets [30]. In order to have a confidence interval of maximum 0.01 pixel (spatial resolution 0,28 mm^2), the correlation criterion "normalized sum of squared differences" was used for image processing. Then, different quantities such as displacements and deformations were evaluated at different points of the wall for different stages of the test.

3.2 Results

The results of the compression tests carried out on the masonry wallets are reported in **Table 2**. The vertical strain and stress variation during the loading protocol is illustrated in **Fig. 4 (a)**. When compared to the constituents ($E_{\text{brick}} = 4362$ MPa), both specimens showed low values of Young's modulus and Poisson's ratio. This difference of rigidity between the constituents and masonry may be explained by the influence of the interface as masonry resistance is strongly related to the tensile bond strength between the joints and the units [31]. In turn, compressive strength of both specimens was approximately the strength of the mortar sample with an aspect ratio of 1 (2.2 MPa). However, it was substantially different from bricks' compressive strength.

Both wallets presented a failure mode characterized by vertical cracks crossing the bricks and the joints. In the MC-1 sample, cracks appeared on one flank of the wall where the bricks eventually detached from the structure (cf. **Fig. 4 (d)**). In MC-2, the main cracks occurred on both sides of the specimen. Besides, a longitudinal and transverse expansion at the top of the wall was noticed. Similar behavior of the masonry was observed by Miccoli et al. [27] after completing uniaxial compression tests on earth masonry wallets, obtaining compression strength values between 2.7 and 3.8 MPa and a Young's modulus of 803 MPa.

Table 2. Mechanical parameters of masonry according to EN 1052-1

Specimens	Dimensions (mm)	F_{max} (kN)	f (MPa)	$\varepsilon_{yy\ 1/3}$ (µm/m)	$E_{1/3}$ (MPa)	$\nu_{1/3}$ (-)
MC-1	525 x 445 x 105	116.0	2.5	2153.7	384.4	0.05
MC-2	570 x 450 x 105	96.4	2.1	1261.4	538.9	0.04

Table 3. Mechanical parameters of masonry according to **Fig. 4**

Specimen	E (MPa)	Eh (MPa)
MC-2	≈ 700	2770

Fig. 4 (b) shows the vertical strain stress curve obtained from the stereo correlation data, with the curves obtained during the load-discharge cycles (LVDT, load cell) used to determine the modulus of elasticity of the MC-2 wall (cf. **Table 3**). In the elastic domain of masonry, the slope of the curves representing the last two charge-discharge cycles (cycles 2 and 3) and the slope of the initial part of the curve calculated through the stereo data correlation are similar. This slope, of approximately 2770 MPa, represents the initial tangent modulus of elasticity of the masonry. This is typical behavior of a plastic soil. Indeed, one can observe the residual strain during the cycles 2 and 3 and the increase of the modulus due to pore closure. **Fig. 4 (c)** shows the evolution of MC-2 vertical deformation field for different compression stress values (after the cyclic modulus loading). During the first three measuring zones, the deformations evolved almost uniformly along the surface of the wall (cf. **Fig. 4 (c)**). For the last measurement point (IV) the most important deformations were concentrated at the bed joints near to the top of the wall and on the left side of the image. Besides, for this stress level, a compressed zone at the bottom left of the wallette can be perceived. As shown in **Fig. 4 (c)**, results can be associated with the failure zones observed at the end of the test. It is interesting to note that the successive appearance of these damaged zones is reflected by an elastoplastic behavior; the failure is concentrated on the left side of the specimen due to a slight asymmetry in the loading between the left and right side. Indeed, for the maximal vertical stress, deformation on the left side was near to one to three times more important than deformation on the right side.

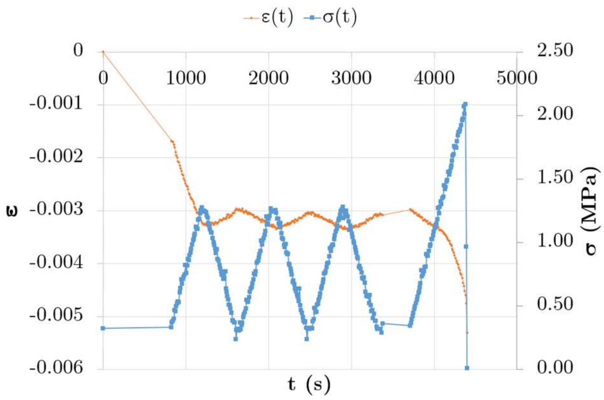

(a)

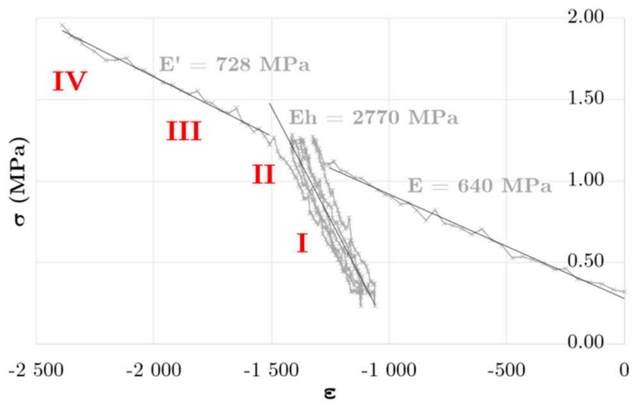

(b)

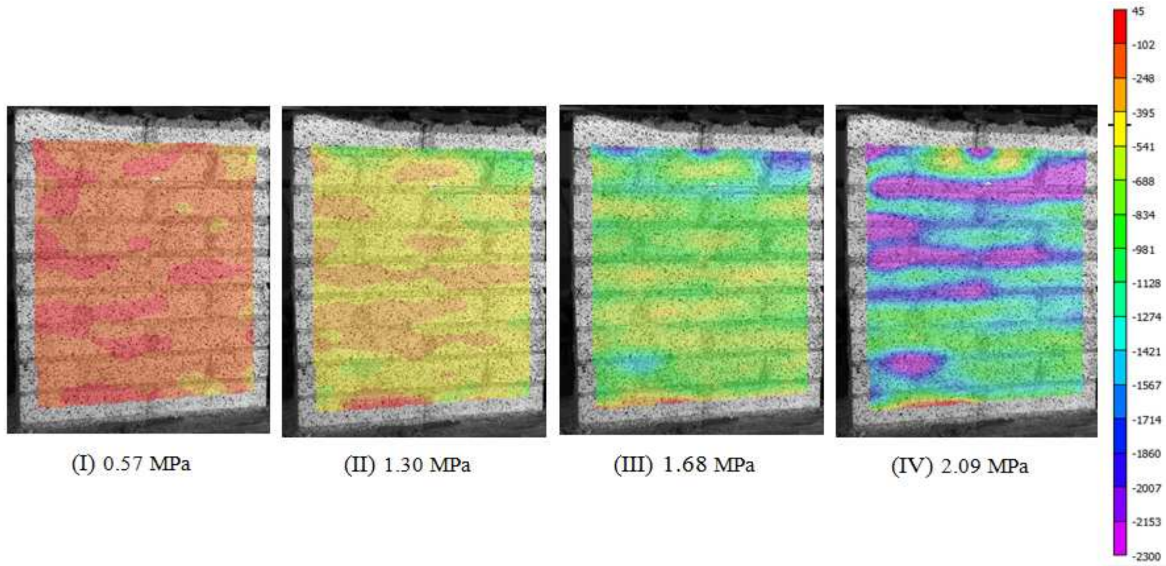

(c)

(d)

Fig. 4 MC-2 test description; (a) loading protocol, (b) vertical strain stress curve obtain throw DIC (c) Evolution of deformation field ε_{yy} [μm/m] for different compressive stress (d) Compression test on masonry.

4 Element of shear wall

Previous section allowed us to evaluate an elementary assembly of the components studied in the first part. Thus, we highlighted that the monotonous uniaxial loading behavior of masonry depends on the behavior of the elements interface. The subsequent study of reinforced and unreinforced shear walls submitted to lateral, cyclic, quasi-static loading will allow studying the crack patterns on a scale representative of the structure.

4.1 Experimental Setup

Two adobe masonry walls were built as depicted in **Fig. 5 (a)** and **(b)**: one was not reinforced (UW, $1.27 \times 1.31 \times 0.34\ \mathrm{m}^3$), the other one (RW, $1.33 \times 1.29 \times 0.34\ \mathrm{m}^3$) was reinforced with a ladder-shaped, horizontal timber insertion. The UW and RW walls were built on welded steel beams. Each wall was built following an "English" masonry building technique. This bond was chosen to be representative of one of the multiple techniques used to lay units on earth masonry buildings [24]-[25]. The longitudinal sections of timber beams had dimensions of $75 \times 45\ \mathrm{mm}^2$, and the transversal ones of $50 \times 45\ \mathrm{mm}^2$, according to the Nepalese design catalogue DUDBC [14]. The pine timber had a C18 mechanical class according to [17]. Longitudinal and transversal elements were connected with screws (diameter 5 mm, length 70 mm) to limit the energy dissipation in the timber-timber connections in order to ease the analysis of the global energy dissipation mechanism in the wall.

A speckle was created on one side of each specimen to prepare the surface of the walls for image correlation analysis. In order to obtain a uniform distribution of the charges applied to the samples, a layer of mortar was extended at the top and on the sides of the walls. Then, a steel piece (in red in **Fig. 5 (c)**) was placed on the top of the wall to ensure the interface between the structure and the machine. Finally, the walls were positioned on the testing machine where adjusting shims were installed to avoid rigid body movement and reduce the duration of the test.

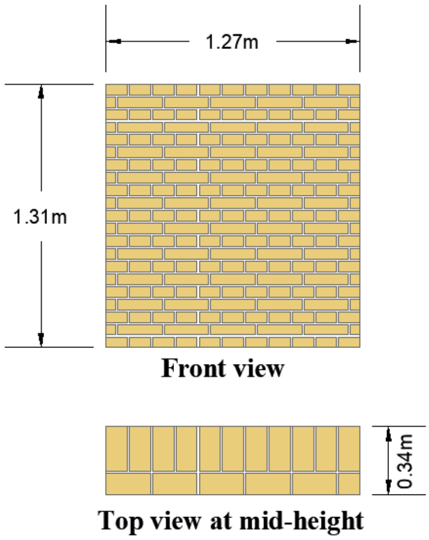

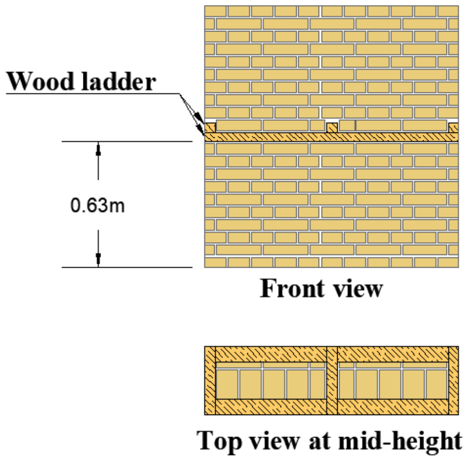

(a) (b)

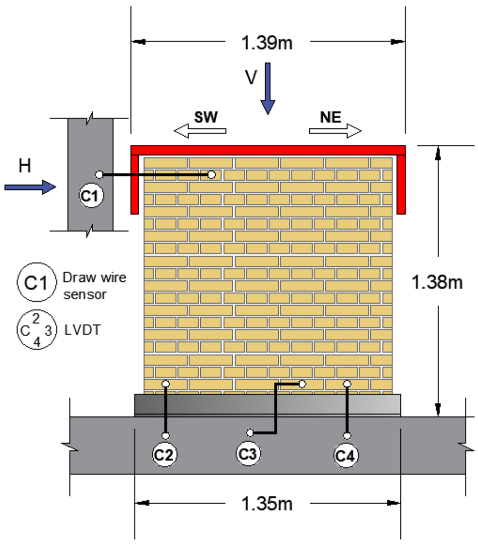

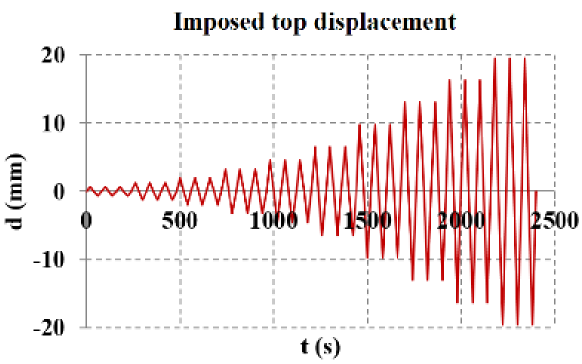

(c) (d)

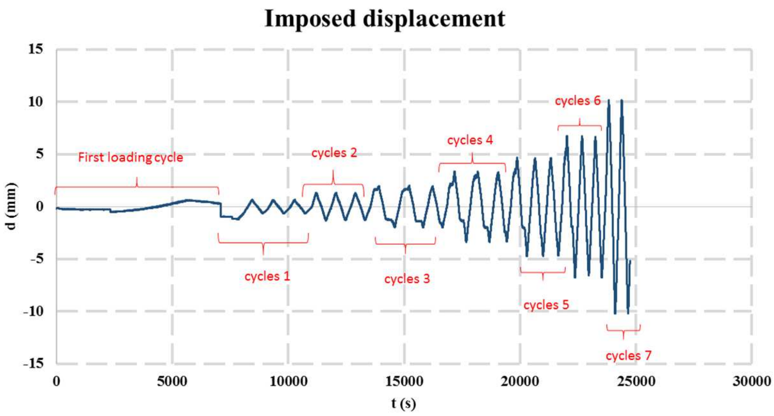

(e)

Fig. 5 Front view and top view at mid-height of unreinforced and reinforced specimens; (a) UW, (b) RW (c) Test setup (d) Imposed top displacement (e) Total imposed displacement.

The tests were performed using a press equipped with a vertical hydraulic actuator to apply compressive loads and a horizontal hydraulic cylinder to impose cyclic loads. Displacements were measured through digital image correlation (DIC) thanks to a stereo-camera system, completed by three LVDT sensors, and a draw wire sensor (cf. **Fig. 5 (c)**). To simulate permanent loads and the presence of stories in such structures, a constant vertical load of 0.2 MPa corresponding to 10% of the compressive strength of the masonry (determined from wallet scale) was applied on top of the walls. The compression is equivalent to the sum of the load of two wooden floors and a distributed occupancy load calculated following the Nepal National Building Code [32]. Vertical load was kept constant during the test by means of the vertical hydraulic actuator piloted in force. The lateral load was applied under imposed displacement designed according to the standard ASTM E2126-05 [33] (cf. **Fig. 5 (d)**). The control displacement curve was made of series of three cycles at a constant frequency (0.013 Hz), with a constant magnitude inside a series, but with increasing magnitude between two series. The real displacement imposed to the wall was actually different due to a problem during the first part of the loading path (cf. **Fig. 5 (e)**).

The displacement measurements of the sensors integrated in the walls (C1, C2, C3 and C4) were compared with the corresponding displacements obtained through the CIN system. To this end, seven fictitious study points (P1 to P7) were defined at several points of the walls. Moreover, two virtual extensometers (E1) were used to measure the deformation along a diagonal reference line (cf. **Fig. 6**). The positioning of the virtual sensors has been chosen so as to obtain representative information for the critical zones, i.e. the diagonals, the center and the base of the walls.

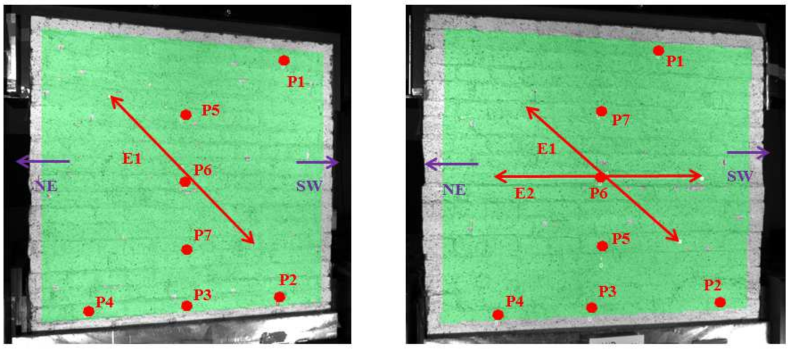

(a) **(b)**

Fig. 6 Reference points and virtual extensometers for; (a) UW, Left, (b) RW, Right.

4.2 Results

Fig. 7 compares the DIC horizontal displacement measurements at point P1 of the UW with the corresponding displacements measured by the physical sensor C1. A noticeable concordance between the two displacement measurements of two systems is obvious. Because the physical sensor and the results of the DIC are not obtained on the same face of the wall, slight differences exist.

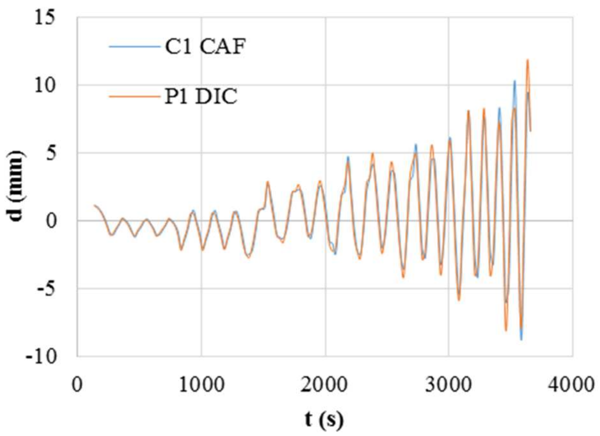

Fig. 7 Virtual CIN and C1 sensor displacement comparison.

Fig. 8 shows the horizontal displacement field obtained by DIC with VIC3D software in the reinforced and unreinforced masonry walls before failure. In the case of the unreinforced masonry adobe wall (UW) (**Fig. 8 (a)**), contours show a typical diagonal crack pattern where negative displacements indicate a left displacement whereas positive values refer to right one. The contours of the reinforced shear wall (RW) (**Fig. 8 (b)**) show the apparition of a friction plane along the bed joints. Two types of failure can be observed here. The unreinforced wall experienced shear failure, according to the presence of diagonal cracks in the joints and through some adobe units. During the first cycles of the quasi-static test, the horizontally reinforced wall showed a behavior similar to the first wall: diagonal cracks appeared at the corners of the wall. However, when the lateral force magnitude increased, a horizontal failure plane developed two beds of bricks below the timber insertion and sliding occurred along this plane. Additionally, very few cracks appeared above the reinforcement.

The inclusion creates a supplementary interface that limits the displacements of the adjacent elements; this apparently reduces the total number of cracks on the element and restrains the crack propagation to certain zones of the wall. Furthermore, the absence of cracks on the first bed of bricks below the timber insertion could be caused by a prestressed state of these elements due to shrinkage of timber during the drying process.

The hysteresis curves lateral force against displacement, corresponding to the quasi-static cyclic tests on UW and RW, are presented in **Fig. 9.** The envelope corresponds to the points of maximal force and maximal displacement for each series of three cycles of same magnitude. One can see that UW depicts an asymetrical behavior due to the initial monotonic loading before the cycles (cf. **Fig. 5 (e)**). During this step, the strength of the wall in the pulling state was reach and it explains why the behavior is close to perfect elasto-plastic.

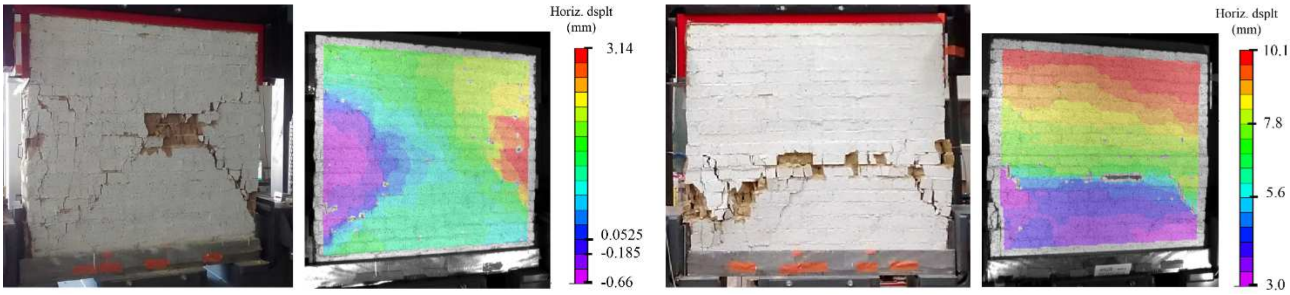

(a) **(b)**

Fig. 8 Horizontal displacement field obtained with DIC and failure pattern: (a) UW, (b) RW.

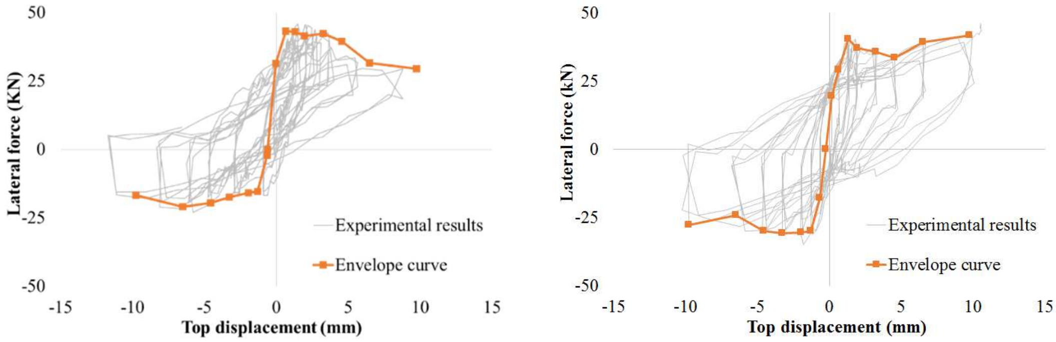

(a) **(b)**

Fig. 9 Hysteresis curves lateral force agaimst displacement for quasi static cyclic tests on: (a) unreinforced masonry shear wall, (b) timber reinforced masonry shear wall.

The use of force-displacement curves is often based on an idealization that transforms these graphs into bilinear envelopes representative of perfectly elastic linear behavior (cf. **Fig. 10 (a)**). In the literature it is possible to find many examples of the application of this method for the analysis of structures seismic response [34]-[36]. From the bilinear representations in push and pull states, the average bilinear idealization for each of the walls was determined. The results are shown in **Fig. 10 (b)**. The RW shows a higher maximum resistance (32.6 kN) and ultimate displacement (9.8 mm).

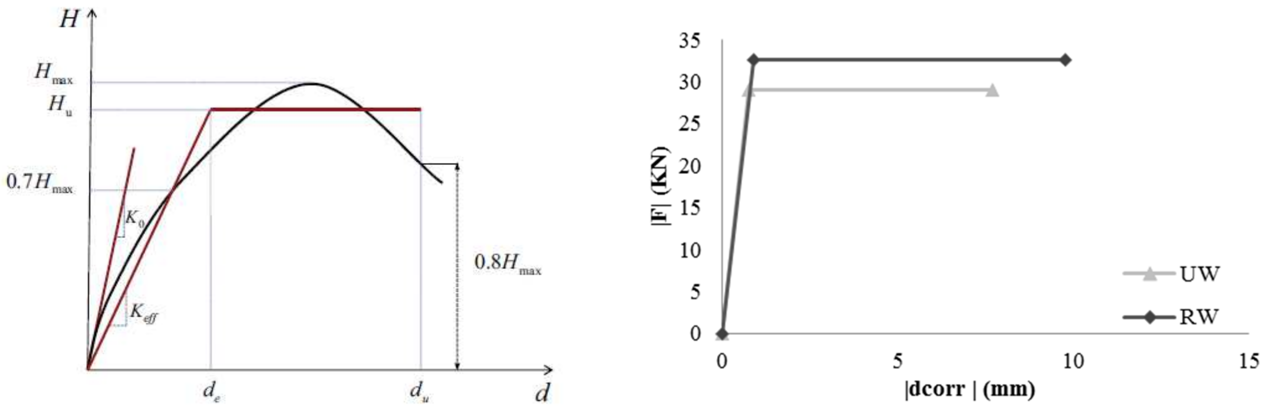

(a) **(b)**

Fig. 10 Bilinear idealization of the hysteresis envelope: (a) critical parameters on seismic behavior analysis [36] (b) idealization for UW and RW.

Table 4 lists the different critical parameters evaluated for each wall. The most notable difference between the two specimens is found in the displacement corresponding to the maximum resistance d_{Hmax}. Indeed, in the case of the UW, H_{max} was reached for a much smaller displacement (1.26 mm compared to 10 mm of the RW wall). However, in general the behavior of the two walls is similar with higher resistances in push state than in pull state and effective stiffness rounding 40 kN / mm. In addition, the RW shows a slight increase in ductility against the UW.

Table 4. Lateral resistance and deformability parameters of UW and RW walls

Test	H_{max} (kN)	d_{Hmax} (mm)	K_{Hmax} (kN/mm)	H_{cr} (kN)	d_{cr} (mm)	K_{eff} (kN/mm)	H_u (kN)	d_u (mm)	d_e (mm)	μ (-)
UW-push	43.32	1.26	34.37	30.32	0.55	55.13	38.99	6.20	0.71	8.77
UW-pull	20.99	5.89	3.56	14.69	0.60	24.49	18.89	9.16	0.77	11.87
Average	32.15	3.58	18.96	22.51	0.58	39.81	28.94	7.68	0.74	10.32
RW-push	41.86	10.00	4.18	29.30	0.90	32.56	37.67	10.00	1.16	8.64
RW-pull	30.51	3.00	10.18	21.36	0.55	38.83	27.46	9.50	0.71	13.43
Average	36.19	6.50	7.18	25.33	0.73	35.69	32.57	9.75	0.93	11.04

Stiffness degradation of the walls was evaluated by computing the slope between two points of maximal force and displacement of two loading series, which corresponds to the slope between two points of the hysteresis curves. Loss of rigidity is widely used as an indicator of the seismic performance of a structure. This parameter depends on characteristics of the structure as well as on the loading history. The stiffness degradation curves (cf. **Fig. 11 (a)**) reveal similar responses for the two walls. Most of the degradation happens during the three first loading cycles, and then the stiffness stabilizes. It can be noticed that the stiffness of the reinforced shear wall degraded slightly more progressively, which fosters the hypothesis of a more ductile behavior of reinforced masonry pointed out by the hysteresis curves.

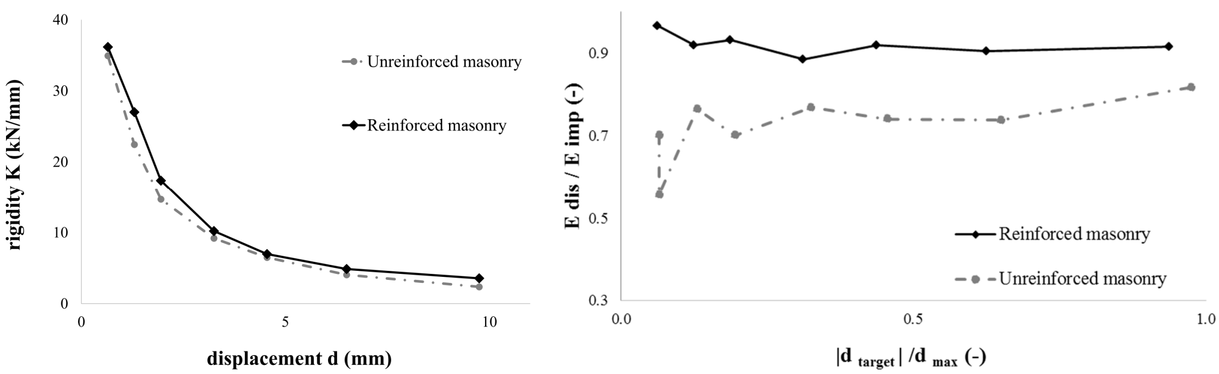

(a) (b)

Fig. 11 (a) Stiffness degradation, (b) Energy dissipation.

The hysteresis curves also reveal some information about dissipated energy in the system. The dissipated energy E_{dis} is defined as the area inside a cycle of hysteresis. The input energy E_{inp} is defined as the area under the curve, down to the x-axis [37]. **Fig. 11 (b)** presents the variation of the ratio E_{dis} / E_{inp} according to the displacement, normalized with the value of maximum displacement during the test d_{max}. The plot shows more significant energy dissipation in the case of the timber reinforced masonry wall (90 %) compared to the unreinforced wall (80 %). This could be explained by the friction phenomenon which is probably more important for the crack pattern depicted in **Fig. 8 (b)**.

Table 5 records the energies E_{inp} and E_{dis} for the first charge cycles of the series of three cycles applied for each target displacement. The supplied energy values and the energy dissipation ratio E_{dis}/E_{inp} are also presented. The first UW cycle (cycle 0) represents the energy values of a preliminary load phase achieved previously to the test. The results show that, for all displacement cycles, the energy dissipated by the RW (E_{dis}) is greater than that of the UW, with a final dissipated energy of 403 kNmm for UW against 627 kNmm for RW. Likewise, it is observed that the energy supplied by the jack to reach the target displacements (E_{inp}) is higher in the case of the RW, with a final supplied energy of 685 kNmm compared to 493 kNmm for the UW specimen.

Results show that the inclusion effect on the stiffness degradation is not significant; however it makes masonry more ductile, giving it a greater energy dissipation capacity, which highlights the importance of using this kind of reinforcement system in structures located in seismic zones.

Table 5. Energy supplied and energy dissipated for each charge cycle

Specimen	Cycle	d target (mm)	d target /d max	E dis (kN mm)	E inp (kN mm)	Edis/Eimp
UW	0	0.65	0.07	24.02	34.22	0.70
	1	0.65	0.07	37.18	66.71	0.56
	2	1.30	0.13	94.91	124.14	0.76
	3	1.95	0.20	107.19	152.93	0.70
	4	3.25	0.33	174.29	226.92	0.77
	5	4.55	0.46	204.52	276.31	0.74
	6	6.50	0.65	244.95	332.15	0.74
	7	9.75	0.98	402.85	492.95	0.82
RW	1	0.65	0.06	31.63	32.74	0.97
	2	1.30	0.13	80.38	87.36	0.92
	3	1.95	0.19	140.60	150.88	0.93
	4	3.25	0.31	179.71	202.83	0.89
	5	4.55	0.44	264.63	287.99	0.92
	6	6.50	0.63	365.77	403.93	0.91
	7	9.75	0.94	626.96	684.68	0.92

5 Conclusions

The results discussed on the scale of the materials highlight the inherent difficulties to characterize the compression strength of earth material. Indeed, this mechanical parameter is highly influenced by the geometry of the samples and by the different properties of the materials used during the tests. Results show that the compressive strength of the bricks increases for a decreasing aspect ratio. Furthermore, it seems that the failure mode depends on the specimen preparation, since only entire bricks tested vertically exhibited the characteristic compression failure mode (two opposite confinement cones), with a relatively low standard deviation that let one think that these tests are the more relevant in the current case. The main limitation for using this test is the geometry of the brick. Regarding the test on stacked bricks, the greater lateral strain of the sand under compression might be the cause of the reduced strength obtained. For the earth mortar, it seems possible to estimate a representative compressive strength, since an aspect ratio of 1 allows achieving the typical compression failure mode. Complementary tests might be performed regarding the stacked bricks configuration since it gives results independent from bricks dimensions.

The compressive strength test performed on the masonry revealed a typical compression failure mode, characterized by the appearance of vertical cracks through bricks and joints. Rigidity difference between elements and masonry highlighted that the monotonous uniaxial loading behavior of masonry depends on the behavior of the elements interface. In turn, the use of a stereovision system completes the understanding of masonry mechanical behavior as it allows the tracking of deformation and strain fields through time, and the tracing of the first cracks formation and its propagation. Moreover, it provides complementary data to the more classical measurement systems.

Experimental results show significant differences concerning the behavior of the walls. The unreinforced wall presents a shear failure, with the development of a diagonal crack pattern following the joints and going through some units. The reinforced wall failure was characterized by the propagation of diagonal cracks at the bottom corners in the beginning of the test, followed by the formation of a horizontal crack below the insertion and the appearance of a sliding surface between the top and the bottom part of the wall. It was noticed that very few cracks developed in the top part of the wall located above the timber reinforcement. Furthermore, the reinforced wall exhibited a more ductile behavior, characterized by greater energy dissipation for higher displacement levels. However, similarly to the unreinforced system, the wall stiffness degrades considerably for the first levels of lateral solicitation. Concerning lateral resistance, reinforced and unreinforced systems revealed similar results.

The inclusion allows limiting the displacements of the adjacent elements which apparently reduces the total number of cracks in the masonry when subjected to lateral forces. Furthermore, timber seems to create a prestressed state on the bed of bricks below the timber insertion, which restrains the crack propagation to certain zones of the wall subjected to ordinary stress conditions. This last feature may limit the risk of collapse of the entire structure when subjected to lateral loads. The overall behavior of reinforced wall highlights the role and the importance of using horizontal timber insertions in masonry structures in seismic zones.

The digital images stereo-correlation is a powerful tool which allows identifying some critical parameters in the response evaluation of the walls under horizontal quasi-static loading. In particular, this system provides information on the moment of first cracks formation, the cracks propagation during the test, and the history of deformations and strain fields. Moreover, the DIC facilitates analysis of results as data is presented through images. However, the accuracy of the results obtained through this technique depends directly on the quality of the recorded images, therefore, a correct acquisition system calibration is critical.

A perspective of the present experimental results is the study of the development of a computational model of the timber reinforced shear wall (see [38]). The current knowledge of the mechanical properties of the elements and of the masonry is a solid base to determine the parameters of a homogenized constitutive law of the earth masonry. A further study of the interface between timber and masonry is also needed to have a proper understanding of the reinforced wall behavior.

6 Acknowledgments

The authors wish to thank and acknowledge the support of the LMDC. Gratitude is extended to C. Soula, L. Delbreil and S. Dos Santos for their valuable assistance during the experimental program.

7 References

[1] CRETE, E., YADAV, S., SIEFFERT, Y., et al (2018) Promoting vernacular architecture as a basis for Building Back Safer: case study: Nepal, 11th International Conference on Structural Analysis of Historical Constructions.

[2] GAUTAM, D., RODRIGUES, H., KUMAR, K., et al (2016) Common structural and construction deficiencies of Nepalese Buildings, *Innovative Infrastructure Solutions*, p. 1-18.

[3] ORTEGA, J., VASCONCELOS, G., RODRIGUES, H. et al (2017) Traditional earthquake resistant techniques for vernacular architecture and local seismic cultures: A literature review, *Journal of Cultural Heritage*.

[4] INAN, Z. (2014) Runner beams as building element of masonry walls in Eastern Anatolia, Turkey *in* Vernacular heritage and earthen architecture: contributions for sustainable development, Taylor & Francis Group, London, UK, p. 721-726.

[5] LANGENBACH, R. (2009) Don't Tear it Down! Preserving the Earthquake Resistant Vernacular Architecture of Kashmir, Oinfroin Media, Oakland, California, p. 21-30.

[6] VINTZILEOU, E. (2008) Effect of timber ties on the behavior of historic masonry. *Journal of Structural Engineering*, Vol. 134, No. 6, p. 961-972.

[7] VIEUX-CHAMPAGNE, F., SIEFFERT, Y., GRANGE, S., et al. (2014) Experimental analysis of seismic resistance of timber-framed structures with stones and earth infill, *Engineering Structures* 69, p. 102–115.

[8] HOFMANN, M. (2015) Le facteur séisme dans l'architecture vernaculaire. Un décryptage entre déterminants culturels, types de structures et ressources cognitives parasismiques PhD thesis. Lausanne: École Polytechnique Fédérale de Lausanne, p. 111-120.

[9] LIU, B.Y., et al. (2006) Damage of village buildings in recent Yunnan earthquakes. The 4th International Conference on Earthquake Engineering, 12-13 octobre 2006, Taipei, Taiwan.

[10] LANGENBACH, R. (2003). "CROSSWALLS" INSTEAD OF SHEARWALLS. In Proceedings of the Turkish Fifth National Conference on Earthquake Engineering, Istanbul, pp. 26-30.

[11] YADAV, S., SIEFFERT, Y., CRETE, E., et al. (2018) Mechanical behaviour of different type of shear band connections being used in reconstruction housing in Nepal, *Construction and Building Materials* 174, p. 701-712.

[12] MACABUAG, J., GURGAIN, R., Bhattacharya, S. (2012) Seismic retrofitting of non-engineered masonry in rural Nepal, *Structures and Buildings* Volume 165 Issue SB6.

[13] SILVA, B., DALLA BENETTA, M., DA PORTO, F., et al. (2014) Experimental assessment of in-plane behaviour of three-leaf stone masonry walls, *Construction and Building Materials* 53, p. 149–161.

[14] Design catalogue for reconstruction of earthquake resistant houses, Department of Urban Development and Building Construction, Ministry of Urban Development, Government of Nepal, Babarmahal, Kathmandu, 2011.

[15] FERREIRA MENDES M. (2015) Support to the Swiss Red Cross for reconstruction in Nepal, June-July 2015 Field Mission Report.

[16] AUBERT, J.E. (2013) Caractérisation des briques de terre crue de Midi-Pyrénées. Rapport final du projet TERCRUSO. p. 11.

[17] ANFOR. *Bois de structure - Classes de résistance.* NF EN 338, La Plaine Saint-Denis : ANFOR, Juillet 2016.

[18] SILVEIRA, D., VARUM, H., COSTA, A. (2013) Influence of the testing procedures in the mechanical characterization of adobe bricks. *Construction and Building Materials*. Vol. 40, p.719–728

[19] AUBERT, J.E., MAILLARD, P., MOREL, J.C., et al. (2016) Towards a simple compressive strength test for earth bricks? *Materials and Structures*, Vol. 49, p. 1641–1654.

[20] ANFOR. Méthodes d'essai des éléments de maçonnerie - Partie 1 : Détermination de la résistance à la compression. NF EN 772-1, La Plaine Saint-Denis : ANFOR, Décembre 2015.

[21] ANFOR. Blocs de terre comprimée pour murs et cloisons : définitions - Spécifications - Méthodes d'essais - Conditions de réception. XP P13-901, La Plaine Saint-Denis : ANFOR, Octobre 2001.

[22] ANFOR. Essais pour béton durci - Partie 3: Résistance à la compression des éprouvettes. NF EN 12390-13, La Plaine Saint-Denis : ANFOR, Novembre 2012.

[23] ANFOR. Méthodes d'essai des mortiers pour maçonnerie - Partie 11 : Détermination de la résistance en flexion et en compression du mortier durci, NF EN 1015-11, La Plaine Saint-Denis : ANFOR, Septembre 2000.

[24] HOUBEN, H., GUILLAUD, H., (2006) *Traité de construction en terre*. 3^{e} edition. Editions Parentheses, Marseille, p. 190-236.

[25] BONAPACE, C., SESTINI, V., (2003) Traditional Materials and Construction Technologies used in the Kathmandu Valley, Paris, November 2003, p. 118.

[26] PKLA, A., MESBAH, A., RIGASSI, V.et al. (2003) Comparaison de méthodes d'essais de mesures des caractéristiques mécaniques des mortiers de terre. *Materials and Structures*, Vol. 36(2), p.108-117.

[27] MICCOLI, L., MÜLLER, U., FONTANA, P. (2014) Mechanical behaviour of earthen materials: A comparison between earth block masonry, rammed earth and cob. *Construction and Building Materials,* Vol. 61, p. 327–339.

[28] AZEREDO, G., MOREL, J-C., BARBOSA, N. (2007) Compressive strength testing of earth mortars. Journal of Urban and Environmental Engineering, Vol.1, n.1, p. 26–35.

[29] AUBERT, J.-E., FABBRI, A., MOREL, J.-C., MAILLARD P. (2013) An earth block with a compressive strength higher than 45 MPa! Construction and Building Materials 47. 366-369.

[30] MOJSILOVIĆ, N., SALMANPOUR, A. (2016) Masonry walls subjected to in-plane cyclic loading: application of digital image correlation for deformation field. *Int. J. Masonry Research and Innovation,* Vol. 1, No. 2, p. 167-187.

[31] LOURENÇO, P. (1998) Experimental and numerical issues in the modelling of the mechanical behaviour of masonry. *Structural analysis of historical constructions II*, CIMNE, Barcelona, p. 58-90.

[32] Government of Nepal, Occupancy Load (Imposed Load) NBC 103: 1994, Babar Mahal, Kathmandu, May 1994.

[33] ASTM, E. 2126-05 (2005) Standard Test Methods for Cyclic (Reversed) Load Test for Shear Resistance of Vertical-Elements of the Lateral-Force Resisting Systems for Buildings. American Society of Testing Materials, 4.

[34] TOMAŽEVIČ, M. (1994) Seismic Behavior of Plain and Reinforced-Masonry Buildings *Journal of Structural Engineering.* Vol. 20, February, p. 323-338.

[35] VASCONCELOS, G., LOURENÇO, P. (2009) In plane experimental behavior of stone masonry walls under cyclic loading. *Journal of Structural Engineering*, Vol. 135, No. 10, October, p. 1269-1277.

[36] SALMANPOUR, A., MOJSILOVIC, N., SCHWARTZ, J. (2015) Displacement capacity of contemporary unreinforced masonry walls: An experimental study: A state-of-the-art review. *Engineering Structures*, Vol. 89, p. 1-16.

[37] TOMAŽEVIČ, M., LUTMAN, M., & PETKOVIĆ, L. (1996). Seismic behavior of masonry walls: experimental simulation. *Journal of Structural Engineering*, 122(9), 1040-1047.

[38] HALA, D., SANTOSH, Y., YANNICK, S., et al. (2019) Damage investigation of adobe walls using numerical simulations. COMPDYN, 7th ECCOMAS Thematic Conference on Computational Methods in Structural

Dynamics and Earthquake Engineering M. Papadrakakis, M. Fragiadakis (eds.) Crete, Greece, 24-–26 June 2019.